



Research article

Dynamic characteristics of CO₂ hydrate formation and spatiotemporal evolution of reservoir parameters during flow processes: Experimental analysis and predictive modeling



Jingru Zhang *, Ke Chen, Guangjun Gong, Yi Zhang *, Yongchen Song **

Key Laboratory of Ocean Energy Utilization and Energy Conservation of Ministry of Education, Dalian University of Technology, Dalian, 116024, China

ARTICLE INFO

Keywords:
CO₂ sequestration
Flow process
Prediction model
Hydrate saturation
Spatiotemporal distribution

ABSTRACT

The hydrate-based geological storage of CO₂ is a highly promising method, wherein CO₂ is injected into a reservoir and flows through it to form hydrates, leading to high density and stable storage. However, the storage capacity cannot be directly measured, and existing research lacks a direct approach to predict the dynamic behavior of CO₂ hydrate formation. In this study, a prediction model for the dynamic formation of CO₂ hydrate and a prediction model for the spatiotemporal evolution of gas pressure and hydrate saturations during flow are presented through experimental studies. Experiments were conducted at different gas flow rates in six cores with different hydrate saturations (19.91%–34.42%). The results revealed a dual-role mechanism of gas flow rate in hydrate formation. Higher flow rates (from 0.03 ml/s to 0.13 ml/s) reduced overall hydrate formation by 40.8% and water conversion by 28% due to shortened gas-water contact time. Conversely, they enhanced nucleation kinetics, decreasing induction time by 71.4% via increased contact frequency. The results elucidate the role of gas flow in porous media in regulating hydrate nucleation and mass transfer, a process insufficiently addressed by conventional kinetic models. Therefore, a dynamic prediction model for hydrate formation was established, expressed as $N(t) = N_0 e^{b/(t + c)}$, which incorporates key hydrate formation parameters and gas flow rate conditions. The predicted values exhibited errors primarily within ±5%. Additionally, our study demonstrated a relationship between hydrate-induced permeability reduction and dynamic inlet pressure evolution. By coupling experimental conditions with permeability models, the spatiotemporal evolution of pressure and hydrate saturation during gas flow is dynamically predicted. This study provides a crucial theoretical foundation for predicting the dynamic behavior of hydrate formation.

1. Introduction

CO₂ geological storage using the hydrate method is a safe, efficient and scalable storage method with significant potential for large-scale application (Macreadie et al., 2019; Sigman et al., 2010; Junji et al., 2023). CO₂ hydrates offer advantages such as high gas storage density, high safety and stability, and diverse storage locations (Zhang et al., 2017). Seabed sediments, deepwater saline aquifers, and terrestrial sedimentary basins are ideal locations for CO₂ geological storage, providing a suitable low-temperature, high-pressure environment for CO₂ hydrate formation (Tongu and Obara, 2024). However, due to the differential distribution of CO₂ gas concentrations and changes in geological structures, CO₂ gas undergoes differential temporal and

spatial seepage, mainly manifested in differences in gas flow rate (Munkejord et al., 2016; Guo et al., 2024). Compared to static conditions, the influence of CO₂ flow behavior on the kinetics of hydrate phase transformation is more complex, with the core issue being the strong coupling between multi-phase non-equilibrium phase transformation and flow-mass transfer-reaction processes (Eigbe et al., 2023a). When gas flow rates exceed a critical threshold, insufficient gas-water contact time can inhibit nucleation (Aminnaji et al., 2024; Yamada et al., 2024). Conversely, too-low flow rates can lead to CO₂ diffusion-dominated regions forming ineffective storage (Kuang et al., 2022; Park et al., 2023). In other words, inappropriate gas flow rates can lead to insufficient gas-water contact time, uneven distribution, and limited heat transfer, thereby reducing the rate and amount of hydrate

* Corresponding author.

** Corresponding author.

E-mail addresses: zhangyi80@dlut.edu.cn (Y. Zhang), songyc@dlut.edu.cn (Y. Song).

formation (Kumar et al., 2024). At the same time, the hydrate formation process can also induce dynamic changes in reservoir characteristics (pressure gradient, porosity, permeability, etc.), which in turn affect other seepage behavior characteristics such as CO₂ gas flow rate (Dashti et al., 2015). In other words, changes in the hydrate itself and changes in reservoir structural parameters have a two-way influence on each other (Lu et al., 2022). Therefore, studying the kinetic behavior of CO₂ hydrate formation at different gas flow rates and the dynamic prediction of reservoir characteristic parameters is of great significance for the optimization and control of CO₂ sequestration strategies.

The kinetic behavior of CO₂ hydrate formation during gas flow under different conditions has been studied. Compared with a stationary system, the characteristic parameters of CO₂ hydrate formation (induction time, formation amount, and formation rate) in a flowing system are more complex, mainly due to the heat and mass transfer behavior between CO₂ flow disturbances and multiphase fluids. The data obtained from the experimental simulation could provide the basis for modeling the kinetics of hydrate formation. To achieve an accurate representation of the kinetic behavior of CO₂ hydrate formation in abandoned gas hydrate reservoirs, Ahmad et al. developed a dynamic mathematical model of coupled mass, momentum, and heat transfer (Ahmad et al., 2020). Englezos et al. proposed the hydrate formation rate prediction equation based on the consideration of fugacity and interfacial mass transfer; the formation rate satisfies $dn/dt = KA(f_b - f_{eq})$ (Englezos et al., 1987). The hydrate formation rate equation proposed by Ahmad et al. is satisfied by $dS_h/dt = K_{exp}e^{-E/RT}[(C_g - C_{ge})]dx$, based on the ideal assumption of a uniform distribution of hydrates (Ahmad et al., 2020). In the above prediction models, although the prediction of the time-varying pattern of hydrate formation can be achieved, there are some problems: (1) there is a theoretical assumption of uniform distribution of hydrate; (2) model parameters such as hydrate area in the prediction model cannot be obtained in real time; and (3) there is no comprehensive consideration of the effect of gas flow rate on hydrate formation. These intractable problems undoubtedly increase the difficulty of predicting the kinetic behavior of hydrate formation under complex conditions.

CO₂ hydrate formation during gas flow has a two-way effect on the spatiotemporal distribution of gas pressure and multiphase fluid saturation in the reservoir. For example, increased hydrate saturation is not conducive to gas diffusion, leading to increased pressure differences in the phase transition reservoir. Appropriate gas-water saturation provides sufficient gas-liquid contact area, which is more conducive to CO₂ hydrate formation. In other words, the quantitative characterization of reservoir parameters (pressure) provides new ideas for dynamic prediction of CO₂ hydrate parameters (saturation, permeability) that cannot be directly obtained. Zhao et al. achieved spatiotemporal prediction of gas pressure during gas hydrate degradation using a modified permeability model (Zhao et al., 2021). Gong et al. developed a permeability model based on measured pressure and flow data. Based on the permeability model, the prediction of hydrate saturation in dissociation reservoirs was achieved (Gong et al., 2024). Unlike methane hydrate dissociation, CO₂ formation behavior is more complex during gas flow. The distribution of gas in porous media is not uniform, and local regional variations in gas concentration can affect hydrate formation (Qi et al., 2023; Weng et al., 2023). In addition, Wang et al. considered capillary forces at the pore scale, modified the methane hydrate decomposition model and achieved predictive analysis of dissociation behavior (Wang et al., 2024). Compared to static systems, temperature and pressure fluctuations caused by flow, along with the complexity of heat and mass transfer, make the hydrate formation process more dynamic and difficult to predict (Gong et al., 2024). Existing studies have primarily focused on predicting characteristic parameters related to methane hydrate dissociation processes or static systems, neglecting the dynamic prediction of hydrate behavior during gas flow processes.

Therefore, this study focuses on the predictive modeling of hydrate dynamics during CO₂ gas flow and the spatiotemporal prediction of gas

pressure. Hydrate cores were remolded under different CO₂ gas flow rates. The time-varying characteristics of hydrate formation and permeability under different in situ conditions were analyzed. The permeability of hydrate-bearing cores under different in situ flow conditions was measured continuously. A dynamic CO₂ hydrate formation prediction model was then proposed under coupled in-situ conditions. Finally, the spatiotemporal evolution of hydrate saturation and pressure under different influencing parameters during CO₂ hydrate formation was predicted. The results of this study can provide an important theoretical basis for the dynamic prediction of CO₂ hydrate phase transition behavior in the flow system.

2. Experiments

2.1. Apparatus and materials

As shown in Fig. 1, this is an experimental system for studying the time-varying behavior of hydrate formation and permeability during gas flow. The experimental setup mainly included a gas injection system, a hydrate formation and permeability measurement system, a back-pressure control system, a water bath control system, a gas collection system, a data acquisition system, and related accessories. The gas injection system consisted mainly of a CO₂ cylinder and an ISCO gas injection pump. The ISCO gas injection pump was used to inject CO₂ gas from the cylinder at a constant flow rate into the inlet end of the core. The hydrate formation and permeability measurement system mainly consisted of a pressure-resistant stainless steel reactor, which was mainly used to hold the core.

The back-pressure control system consisted of a back-pressure ISCO control pump, a mass balance, and a back-pressure buffer tank. Gas flowing through the outlet end of the reactor first entered the back-pressure buffer tank. The gas flow was then collected by the gas collection system via the ISCO back-pressure control pump. A mass scale was used to weigh the water in the gas stream. The gas collection system mainly consisted of a body collection tank to collect the high-pressure CO₂ gas. The water bath control system consisted mainly of a water bath and a water tank. The water bath was used to control the temperature of the ISCO pump and to hold the reactor to provide a low-temperature environment for hydrate formation. The data acquisition system consisted mainly of a temperature sensor, a pressure sensor, an A/D module, and a computer. The electrical signals collected by the sensors were converted by the A/D module and input to the computer for data recording and processing. The associated accessories included valves, stainless steel pipework, and insulating foam.

The experimental materials used in this study mainly included CO₂ gas, deionized water, and glass sand. The relevant characteristic parameters of the remolded cores and experimental materials are summarized in Table 1.

2.2. Experimental procedure

This study included the key steps of core remolding, hydrate formation, and permeability measurement. The remolded core had a diameter of 5 cm, a height of 6 cm, a porosity of 34.8%, an initial absolute permeability of 12 mD, and a water saturation of 45%.

- (1) Core remolding: 190.5 g of BZ01 glass sand was weighed and placed in a drying oven for 24 h at 373 K to remove water completely. Then, the dried glass sand was evenly mixed with 18.5 g of deionized water and then loaded into the stainless steel reactor in layers. The pipes were connected, and a certain amount of 0.5 MPa of CO₂ was injected to remove the air.
- (2) Hydrate formation: Set the back-pressure valve to a constant back pressure of 3 MPa and opened valves V3 and V2, and injected a large amount of CO₂ gas at a constant flow rate using a high-pressure gas ISCO pump until the pressure in the reactor was

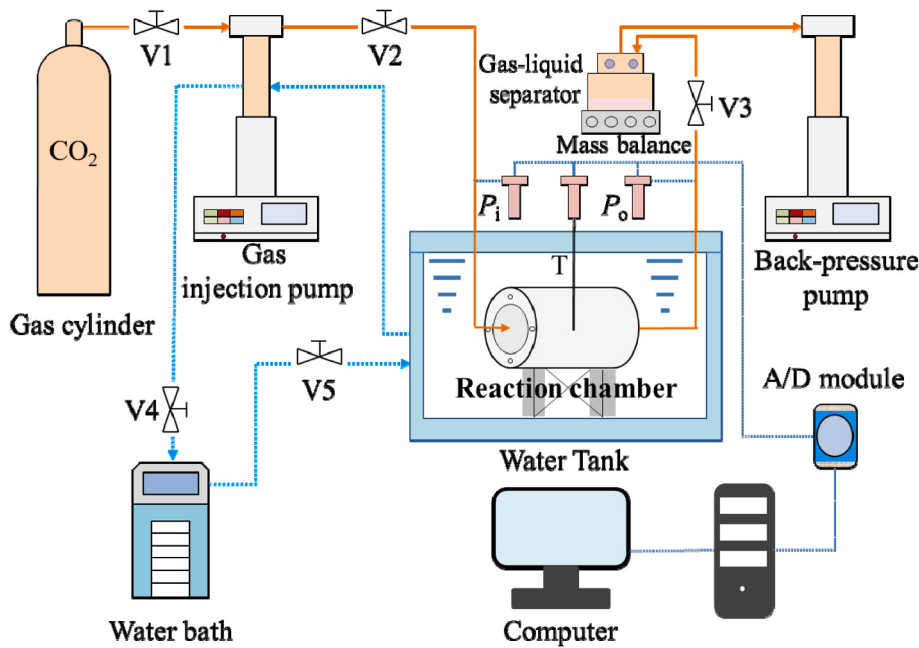


Fig. 1. Schematic diagram of CO_2 hydrate formation and permeability measurement apparatus.

Table 1
Characteristic parameters of remolded cores and experimental materials.

Materials	Parameter	Vendor
Glass sand	BZ01	As-One Co., Japan
Deionized water	Lab-made	Aquapo 2S, Chongqing Ever Young Enterprises, China
CO_2	Purity 99.99%	Dalian Special Gases Co., China

equal to the set back-pressure value. The water bath temperature was set at 276.15 K. After the temperature stabilized, CO_2 gas was injected at different gas flow rates. Hydrate formation was considered complete when the gas pressure of the remolded core no longer changed.

(3) Permeability measurements: A gas flow rate of 0.03 ml/s was injected into the remolded core, and the inlet and outlet pressures at both ends were recorded when the gas flow stabilized. Then, Darcy's law was used to calculate the permeability under different in-situ conditions.

2.3. Data processing

The amount of gas substance (n_g) is calculated from the ratio of the volume of the gas to the product of the specific volume ($\nu(P, T)$) and the molar mass (M_g). The amount of gas substance can be calculated using equation (1).

$$n_g(t) = V_g / (\nu(P, T) \cdot M_g) \quad (1)$$

where V_g refers to the pore volume occupied by the gas within the remolded core.

Hydrate formation is the difference between the injection ($n_{\text{injection}}$) and collection ($n_{\text{collection}}$) of amount of gas substance. The hydrate formation volume can be obtained from equation (2).

$$n_h(t) = n_{\text{injection}}(t) - n_{\text{collection}}(t) \quad (2)$$

Hydrate saturation is the percentage of the pore volume of the remolded core occupied by the hydrate volume, which can be calculated using equation (3).

$$S_h = n_h \cdot M_h / (V_{\text{pore}} \cdot \rho_h) \quad (3)$$

where S_h is the hydrate saturation, V_{pore} is the pore volume of the remolded core, M_h is the molar mass of the CO_2 hydrate, and ρ_h is the density of the CO_2 hydrate. The hydrate number of CO_2 hydrate is assumed to be 6 in this study.

The real-time water conversion rate ($\Phi_{w(t)}$) refers to both the real-time mass of water consumed ($m_{w,t}$) as a percentage of the initial mass of water ($m_{w,0}$). The calculation of the water conversion rate in this study can refer to equation (4).

$$\Phi_{w(t)} = m_{w,t} / m_{w,0} \quad (4)$$

3. Results and discussions

It is more important to study CO_2 hydrate formation during flow than in the static system. This is because formation under flow conditions better reflects the dynamic environment in practical applications, which involves dynamic changes in key factors such as gas injection, reservoir response, and hydrate stability (Yamada et al., 2024). Reservoir and fluid properties, among others, lead to the existence of different gas flow rates within the reservoir, mainly in the range of 0.01–2.5 ml/s (Bashir et al., 2024). Variations in gas flow rate affect the gas-water contact time, mass transfer efficiency, and hydrate formation rate, which in turn affect the amount of hydrate produced and the spatiotemporal distribution of gas pressure (Yin et al., 2018). Therefore, in this study, the behavioral characteristics of CO_2 hydrate formation at different gas flow rates (0.03–0.13 ml/s) were comparatively analyzed. On this basis, coupled with the permeability equation, the gas pressure distribution during the flow process was predicted. The water saturation of the core remolded with glass sand was 45%, and the initial permeability was 12 mD. The specific experimental conditions and results were given in Table 2.

3.1. Dynamic evolution of characteristic parameters of CO_2 hydrate formation at different gas flow rates

A comprehensive understanding of the formation patterns of CO_2 hydrates during the flow process can help optimize injection strategies

Table 2

Experimental condition settings and results.

Case	Gas flow rate (ml/s)	Hydrate formation (mol)	Hydrate saturation	Induction time (min)	Water conversion ratio	Permeability (mD)
1	0.03	0.098	34.42%	35	0.66	4.17
2	0.05	0.094	33.10%	29	0.64	4.39
3	0.07	0.086	29.93%	27	0.58	4.93
4	0.09	0.078	26.77%	21	0.52	5.51
5	0.11	0.066	22.87%	18	0.44	6.27
6	0.13	0.058	19.91%	10	0.38	6.89

and dynamically predict changes in reservoir characteristic parameters (Munkejord et al., 2016). Case 1 is used as an example to illustrate the characteristic behavior of CO₂ hydrate formation during gas flow. The dynamic changes of gas pressure and gas substance amount in the hydrate reservoir during CO₂ flow are illustrated in Fig. 2. As shown in Fig. 2(a), hydrate formation affects the increase of inlet pressure, which also results in the increase of the pressure difference between the inlet and outlet. Hydrate formation significantly reduces the permeability of the reservoir, which is unfavorable to the continuous flow of gas, thus further exacerbating the increase in inlet pressure (Gong et al., 2024). The inlet pressure of the remolded core increases to 3.86 MPa and 4.23 MPa at 300 min and 600 min, respectively. The dynamics of the CO₂ volume during the flow at an injection flow rate of 0.03 ml/s is shown in Fig. 2(b). Before hydrate formation, the injected and collected volumes are kept equal, and the injected gas volume increases linearly with increasing injection time. At 300 min, 450 min, and 600 min, the gas injected into the inlet is 0.91 mol, 1.40 mol, and 1.85 mol, respectively. After 35 min, there is a significant difference between the injected and collected volumes due to hydrate formation. Gas consumption is as high as 0.098 mol at 600 min.

The study of the effect of different flow rates on hydrate formation can help to optimize the economy and safety of geological storage of CO₂ and provide a scientific basis for the optimization of the storage scheme (Eigbe et al., 2023b). The CO₂ hydrate formation curves at different flow rates are summarized in Fig. 3. In general, the hydrate formation has a certain induction time, and the hydrate formation is heterogeneous at different flow rates. Firstly, the induction time of hydrate formation is about 35 min at a gas flow rate of 0.03 ml/s. The induction time of hydrate formation exists because the formation of hydrate needs to reach certain temperature and pressure conditions and undergo the process from dissolution to crystal formation. Secondly, the amount of hydrate formation is inversely proportional to the gas flow rate. Gas flow rates of 0.03 ml/s, 0.05 ml/s, 0.07 ml/s, 0.09 ml/s, 0.11 ml/s, and 0.13 ml/s correspond to hydrate production of 0.098 mol, 0.094 mol, 0.086 mol, 0.078 mol, 0.066 mol, and 0.058 mol, respectively. An increase in gas flow rate usually results in a decrease in the gas-water contact time, which can reduce the chances of the gas combining with water

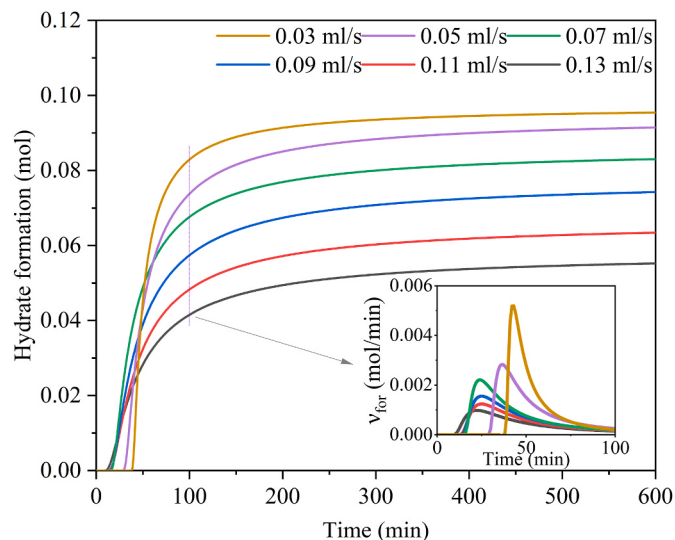


Fig. 3. Time-varying characteristics of hydrate formation at different flow rates.

molecules to form hydrates, which in turn contributes to a decrease in the final hydrate amount (Zhao et al., 2023).

In addition, the hydrate formation rate (v_{for}) is calculated during the first 100 min. The real-time hydrate formation rate is obtained from the tangent slope of the hydrate formation curve. It can be seen from the subplot of Fig. 3 that the maximum CO₂ hydrate formation rate decreases with increasing gas flow rate within 100 min. This is due to the different formation induction times and formation amounts at different gas flow rates. Although the induction time is shortened, the rapid gas flow may cause the local gas concentration to be too low to maintain a high hydrate formation rate, so instead the maximum formation rate decreases at higher flow rates.

A comparison of the parameters characterizing hydrate formation

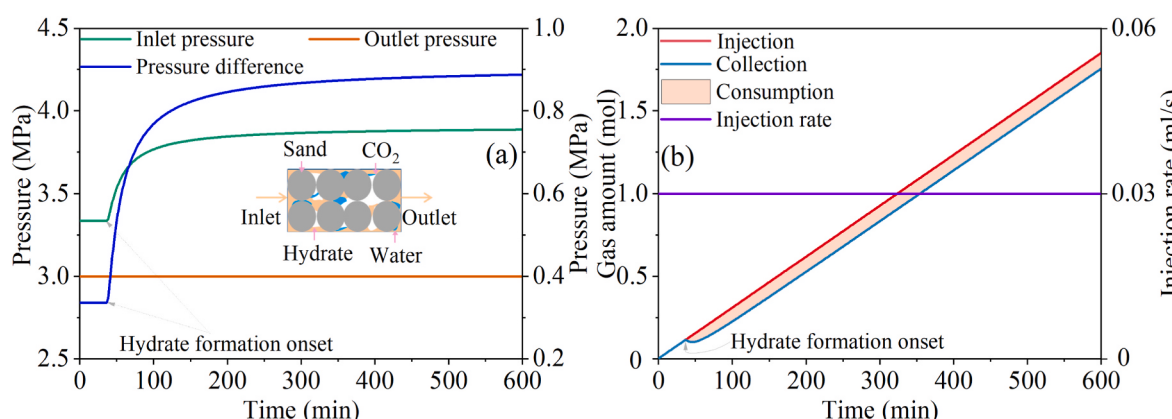


Fig. 2. Time-varying regularity curves of reservoir characteristic parameters during gas flow. (a) gas pressure and differential pressure; (b) gas substance amount and injection flow rate.

(induction time, hydrate formation, and water conversion rate) at different flow rates is shown in Fig. 4. In this study, the hydrate formation induction time is defined as the time corresponding to when the hydrate formation curve starts to increase. For the induction time, the hydrate formation induction time decreases as the gas flow rate increases. The hydrate formation induction times corresponding to gas flow rates of 0.03 ml/s, 0.05 ml/s, 0.07 ml/s, 0.09 ml/s, 0.11 ml/s, and 0.13 ml/s were 35 min, 28 min, 16 min, 14 min, 12 min, and 6 min, respectively. High flow rates may enhance turbulence and mass transfer, increasing local supersaturation and accelerating hydrate nucleation (Ouyang et al., 2024). However, for both hydrate formation and water conversion rate, the increase in gas flow rate shows a decreasing trend for both. When the gas flow rate increases from 0.03 ml/s to 0.13 ml/s, the hydrate formation decreases by 0.04 mol, and the water conversion rate decreases correspondingly from 0.66 to 0.38. At high flow rates, the gas residence time is too short, which may induce strong shear forces that destroy the hydrate membrane, limiting hydrate growth.

3.2. Predictive modelling of hydrate dynamic formation during CO₂ flow and permeability modelling

By quantitatively analyzing the experimental data and coupling the physical data to derive a predictive model, the fundamental laws and kinetic parameters describing the hydrate formation process can be derived, allowing the process behavior to be predicted and optimized under different operating conditions (Mwakipunda et al., 2024). Meanwhile, the introduction of a predictive model for hydrate dynamic formation during CO₂ flow is crucial because the hydrate dynamic formation during CO₂ flow in the reservoir cannot be directly measured in real time. Taking Case 1 as an example, the CO₂ hydrate formation curve at a gas flow rate of 0.03 ml/s is shown in Fig. 5.

Based on the experimental data, a prediction model for the dynamic formation of CO₂ hydrate during gas flow is proposed as equation (5).

$$N(t) = N_0 \cdot e^{b/(t+c)} \quad (5)$$

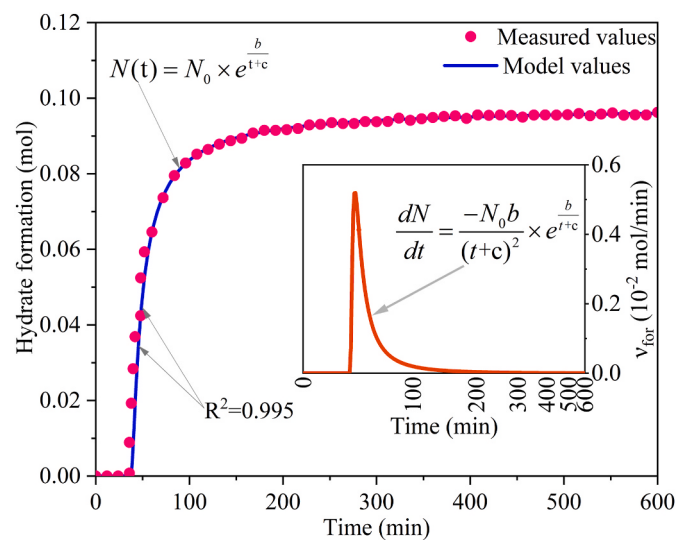


Fig. 5. Typical hydrate dynamic formation curves and prediction models.

where N_0 is defined as the amount of hydrate formation in mol and takes the value 0.098. b and c are defined as time variables related to the gas flow rate in min and take the values -10 and 0.045, respectively. The parameter b reflects the inhibitory effect of gas flow rate on hydrate nucleation. A higher flow rate leads to a larger absolute value of b , indicating a stronger nucleation delay effect. The parameter c characterizes the kinetic transition from a non-equilibrium state to steady-state nucleation during hydrate formation. A higher value of c indicates greater difficulty in reaching the critical nucleation size during hydrate formation. To further validate the correlation between the measured and modeled data, a correlation coefficient (R^2) is introduced. The higher value of which indicates that the model is more predictive of the hydrate formation behavior. In this study, the correlation coefficient between

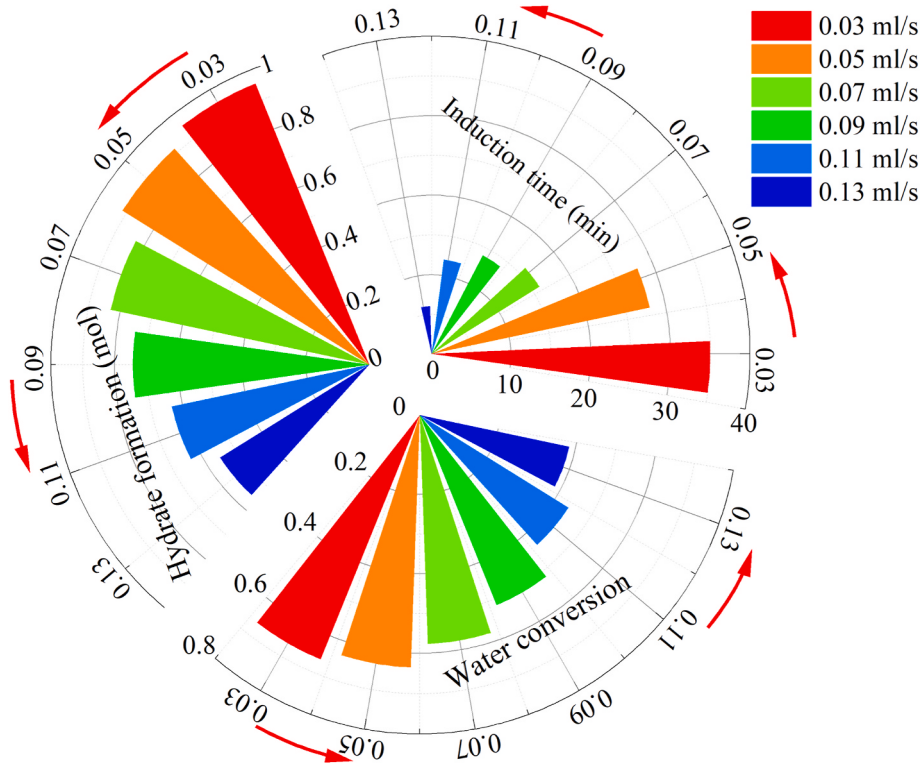


Fig. 4. Comparison of characteristic parameters of hydrate formation at different flow rates.

the measured and modeled data is 0.995. The correlation values of the parameters in the hydrate formation prediction model at different flow rates are summarized in [Table 3](#). It should be noted that the current model is developed based on a gas flow-dominated hydrate formation system in isothermal experimental conditions. The proposed model utilizes core-scale measurement data, while future research will focus on expanding the investigation scale to reservoir conditions, thereby providing crucial theoretical guidance for practical engineering predictions.

Based on equation (5), the hydrate formation rate is calculated. The real-time hydrate formation rate is given by equation (6).

$$\nu_{for}(t) = -N_0 \times b / (t + c)^2 \times e^{b/(t+c)} \quad (6)$$

To further analyze the dynamic variation patterns of each parameter in the prediction model, the values of the parameters taken for different in-situ conditions are shown in [Fig. 6](#). Parameter b decreases with increasing gas flow rate. As the gas flow rate increases from 0.03 ml/s to 0.13 ml/s, the parameter b decreases from -10 to -32 . However, the parameter c increases as the gas flow rate increases. The corresponding values of parameter c are taken as 0.045 min and 0.13 min for the increase in gas flow rate from 0.03 ml/s to 0.13 ml/s. A single linear relationship is maintained between the parameters b , c , and the gas flow rate, which are satisfied by equations (7) and (8), respectively.

$$b = -212.85\alpha Q - 5.80 \quad (7)$$

$$c = 0.89\beta Q + 0.013 \quad (8)$$

where α and β are the correction coefficients for the flow rate in (min·s)/ml, both of which take the value of 1 in this study. By inserting equations (7) and (8) into equation (5), the model for the dynamic formation of hydrate during gas flow is derived for the coupled working conditions.

$$N(t) = N_0 \cdot e^{(-212.85\alpha Q + 5.80)/(t + 0.89\beta Q + 0.013)} \quad (9)$$

To verify the reliability of the predictive model for hydrate dynamic formation, the comparison between the predicted and measured values of hydrate formation at different flow rates is shown in [Fig. 7\(a\)–\(f\)](#). As can be seen from the figure, most of the predicted and measured values in this study are distributed on a straight line with a slope of 1, which directly indicates the good correlation between them. Except for the error interval between measured and predicted values at the 0.05 ml/s gas flow rate, which is distributed within $\pm 8\%$, all others are distributed within a $\pm 5\%$ error interval. In other words, the R^2 between measured and predicted values are all greater than 0.921. To further validate the applicability of the predictive model, we systematically compared its performance with data from Case 1 of [Meyer et al. \(2018\)](#), [Song et al. \(Wang et al., 2018\)](#), and [Gong et al. \(2025\)](#) under varying conditions. As illustrated in [Fig. 7\(g\)–\(i\)](#), the model demonstrates robust predictive capability, with R^2 between measured and predicted values reaching 0.952, 0.934, and 0.923, respectively. The errors between measured and predicted values may be due to the combined effects of experimental errors, parameter uncertainties, system complexity, and differences in experimental conditions ([Stolwijk and Mehrmann, 2018](#)). Different mapping colors in [Fig. 7](#) indicate different hydrate formation amounts, the hydrate formation is distributed in the range between 0 and 0.1 mol.

Table 3

Parameter values of hydrate formation prediction models under different in situ conditions.

Case	N_0 (mol)	b (min)	c (min)
1	0.098	-10	0.045
2	0.094	-18	0.056
3	0.086	-21	0.065
4	0.078	-27	0.098
5	0.067	-29	0.11
6	0.058	-32	0.13

Based on the above analysis, it can be concluded that gas flow rate has a significant impact on the time-dependent characteristics of hydrates. The presence of hydrate will increase the flow resistance of the fluid, which is unfavorable to the time-varying flow of the gas, and consequently affect the inlet pressure ([Gong et al., 2023](#)). As shown in [Fig. 8](#), there is a coupled relationship between gas flow rate, hydrate saturation, and inlet pressure. The inlet pressure of the core in this study increases as the gas flow rate increases. The result of this study has the same phenomenon as the result of [Gong et al. \(2023\)](#). As the gas flow rate increases, the resistance of the gas in contact with the core increases. To maintain a higher flow rate, the gas must overcome greater friction and flow resistance, thus requiring a higher inlet pressure ([Zhu et al., 2022](#)). The inlet pressures at 34.42% hydrate saturation and gas flow rates of 0.03 ml/s, 0.05 ml/s, 0.07 ml/s, 0.09 ml/s, 0.11 ml/s, and 0.13 ml/s are 3.72 MPa, 4.22 MPa, 4.72 MPa, 5.23 MPa, 5.76 MPa, and 6.28 MPa, respectively. Similarly, the inlet pressure of the core increases with the increase in hydrate saturation. The hydrate saturation increases from 19.91% to 34.42% at a gas flow rate of 0.03 ml/s, and the inlet pressure increases from 3.72 MPa to 3.78 MPa accordingly. Overall, the gas flow rate influences the amount of hydrate production in the flow regime, which leads to the dynamic change of the inlet pressure of the core.

The alterations in hydrate saturation have been demonstrated to exert an influence on the dynamics of permeability within remolded hydrate cores, which in turn affects the spatiotemporal distribution of pressure parameters ([Lijith et al., 2024](#)). To conduct a comprehensive investigation into the relationship between hydrate saturation and permeability, the gas permeability of hydrate-bearing cores is calculated using Darcy's law. The average of multiple measurements is used for statistical analysis to reduce the experimental measurement error. The results of this study are illustrated in [Fig. 9](#), which shows the dynamic changes of gas pressure and permeability in Case 1.

During the course of the measurements, minor fluctuations in inlet pressure are observed, with a range from 3.71 MPa to 3.78 MPa being recorded. Concurrently, the outlet pressure is maintained at a constant level of 3 MPa, thereby ensuring stability. These fluctuations in the inlet pressure may be attributed to the coupling between the compressibility of the gas and the resistance to flow, a phenomenon that is to be expected, particularly when the effects of external experimental conditions are disregarded ([Qi et al., 2023](#)). The fluctuation of inlet pressure give rise to a concomitant fluctuation of permeability, which exhibits a main range from 3.79 mD to 4.19 mD. As hydrate saturation increases from 0 to 34.42%, the corresponding permeability measurement is 4.17 mD, which is 7.83 mD lower than the initial permeability. This indicates that the formation of hydrate significantly affects the permeability of the cores and further verifies the inverse relationship between hydrate saturation and permeability.

On the one hand, hydrates occupy the pore space for fluid flow. On the other hand, hydrates themselves have ice-like properties and are impermeable ([Sun et al., 2023](#)). The presence of hydrates significantly reduces the permeability of remolded cores ([Aghajanloo et al., 2024](#)). To further analyze the mutually coupled interaction relationship between hydrate saturation and permeability, the measured data are compared with the classical permeability equation and the modified permeability equation in this study, respectively. The predicted data and measured data of the models with different permeability formulations are counted in [Fig. 10](#).

Firstly, with the increase in hydrate saturation, the permeability shows a decreasing trend. From the measured data, the hydrate saturation increases from 0 to 34.42%, and the permeability decreases by 7.83 mD. Meanwhile, to further obtain the best permeability model formula, the difference between the predicted data and the measured data is intentionally filled by the shaded area in this study. The smaller shaded area indicates that the predicted data can better portray the permeability under different hydrate saturations. The measured data and predicted data in [Fig. 10\(a\)](#) have the lowest shaded area. It also

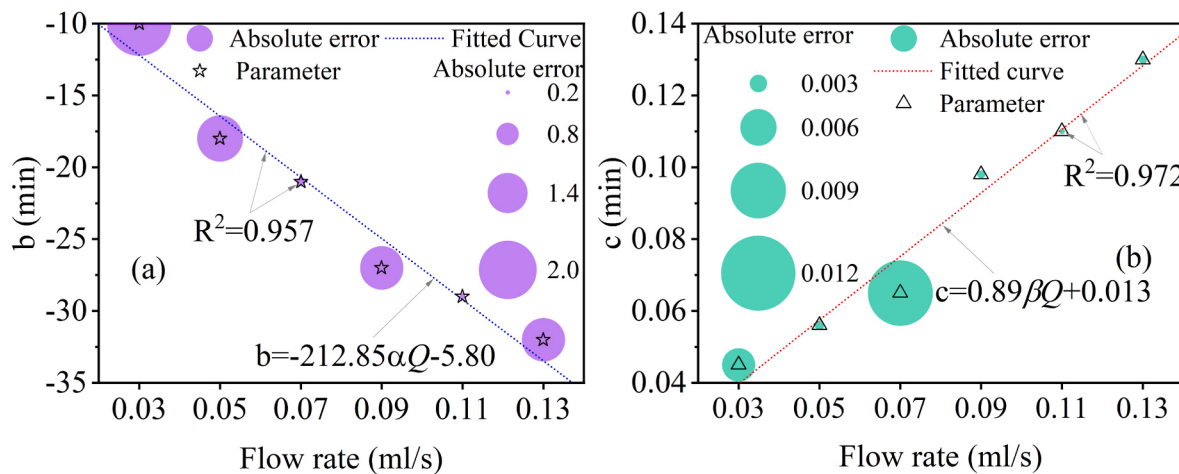


Fig. 6. Distribution of parameter values of hydrate formation kinetic model at different flow rates.

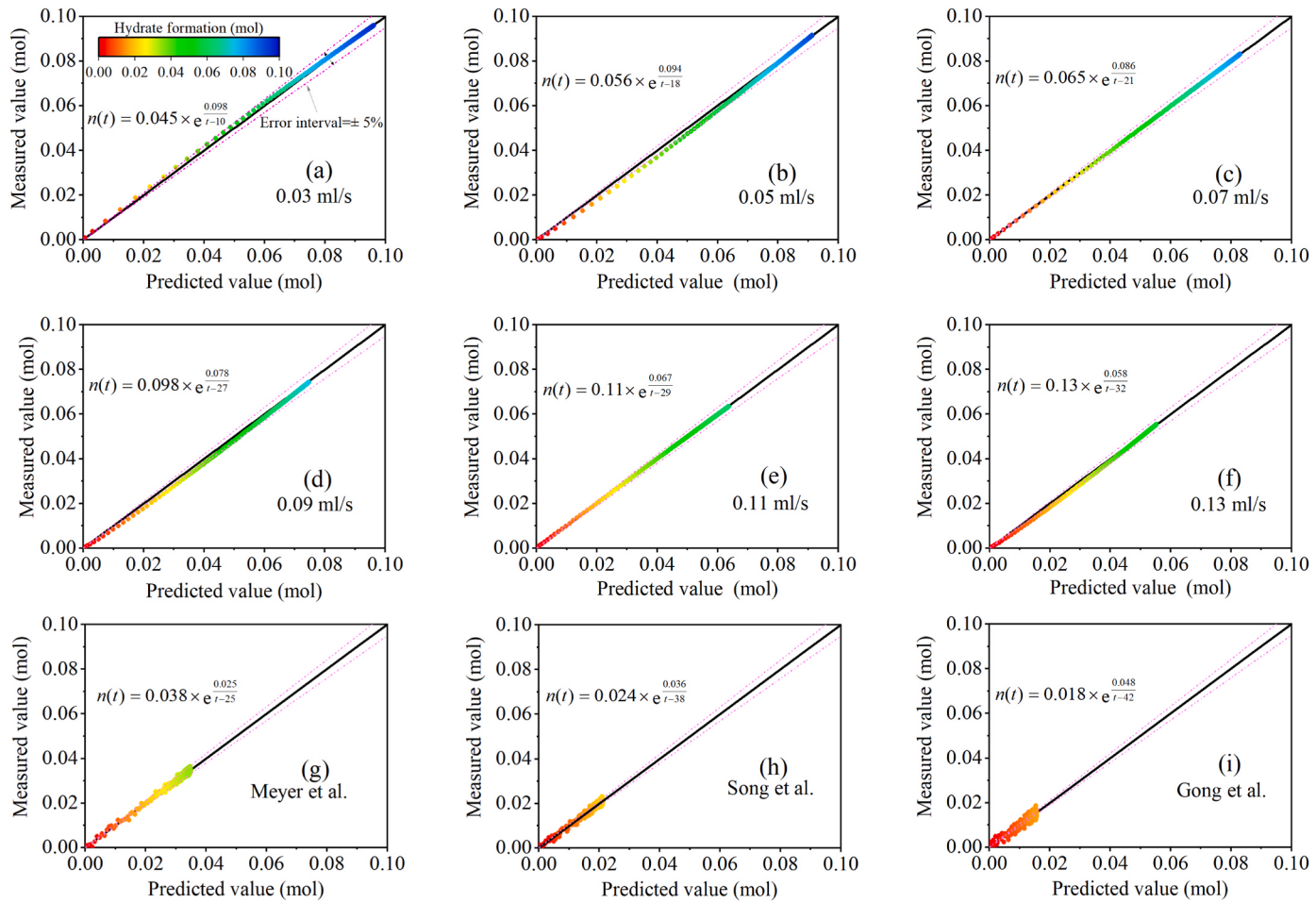


Fig. 7. Comparative analysis of the measured and predicted hydrate formation values: Values obtained from (a)–(f) measurement at 0.03–0.13 ml/s; (g) Ref. Meyer et al.; (h) Ref. Song et al.; (i) Ref. Gong et al.

means that the hydrate saturation-permeability under the conditions of this study better satisfies equation (10).

$$K = K_0(1 - S_h)^{2.5} \quad (10)$$

The permeability (K) in this study refers to the effective absolute permeability under single-phase flow conditions, which is used to evaluate the overall flow capacity and behavior of CO_2 hydrate-bearing

cores. Although local temperature variations may exist due to phase change heat and thermal conductivity differences, their impact on the permeability measurements in this study was negligible and therefore not discussed.

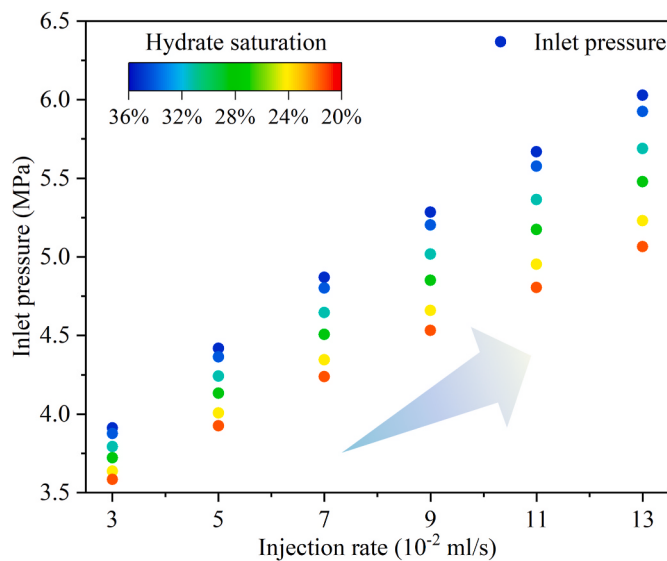


Fig. 8. Relationship between different injection flow rates, hydrate saturation and inlet pressure.

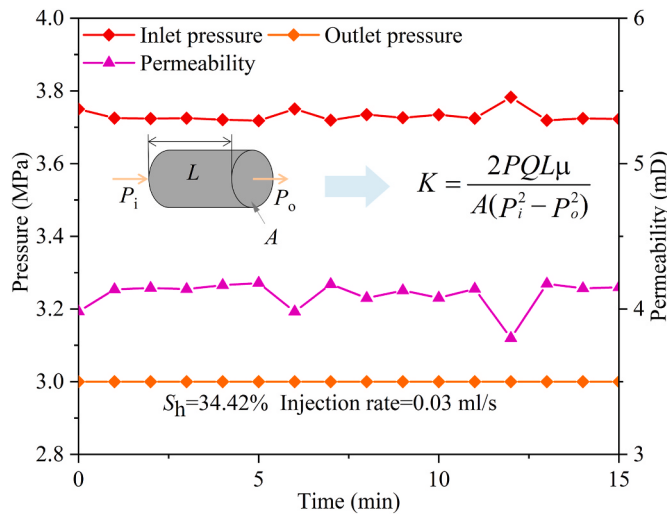


Fig. 9. Dynamic changes in pressure and permeability during permeability measurements of hydrate-bearing cores.

3.3. Characterization of pressure distribution and spatiotemporal prediction of hydrate saturation

The spatiotemporal prediction of reservoir pressure and hydrate saturation during the flow process is imperative for the optimization of the CO₂ storage scheme. The time-varying curve of inlet pressure can be directly obtained in the practical engineering application of CO₂ geological storage by the hydrate method, and key parameters such as gas injection flow rate should be dynamically adjusted to improve the storage rate. As illustrated in Fig. 11, the schematic diagram of the hydrate method CO₂ storage process and key parameters prediction. In the process of CO₂ hydrate formation under different in situ conditions, hydrate saturation is a 'dark box' parameter, which is a physical characteristic parameter that cannot be obtained intuitively (Gong et al., 2024). Combined with the results of the above studies, the dynamic change of hydrate saturation will cause the dynamic change of the inlet pressure of the core. Therefore, coupled with a large amount of experimental data, this study proposes a spatiotemporal prediction of hydrate saturation based on the dynamic change of inlet pressure. By accurately

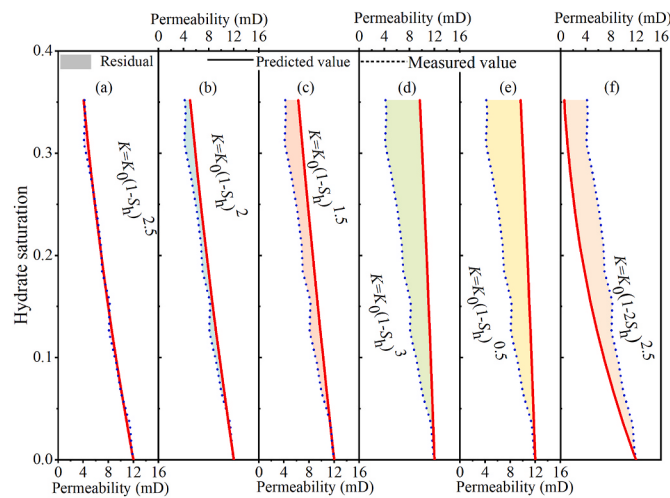


Fig. 10. Comparison of different permeability models with hydrate saturation-permeability.

predicting the hydrate saturation distribution in the reservoir, the efficiency of resource utilization can be improved, the risk of the storage process can be reduced, and the safety and sustainability of the operation can be ensured.

With regard to the dynamic prediction of key parameters (pressure distribution, hydrate saturation) during CO₂ hydrate sequestration, the development process of the relevant mathematical model and the logical reasoning flowchart are summarized in Fig. 12. It should be noted that there are certain theoretical assumptions in this study: (1) the reservoir temperature is assumed to remain constant to simplify the complex heat transfer processes, with primary focus placed on the influence of gas flow on hydrate formation kinetics while neglecting temperature effects on gas flow; (2) the gas flow process is described using the ideal gas equation of state (Gong et al., 2024). Firstly, hydrate saturation and permeability are calculated based on experimentally measured temperature, gas pressure, and gas flow rate. Combined with Darcy's law, the coupling equation between permeability, pressure, and gas flow rate is then obtained. The related coupling relationship can refer to equation (11). Then, coupling the key parameters such as hydrate saturation and absolute permeability, the modified permeability model is established to obtain the permeability-saturation dynamic curves under different in situ conditions. The modified permeability model can refer to equation (10). Furthermore, the permeability equations of the two are established equivalently, and then the dynamic evolution relationship curve between pressure-saturation-flow rate is obtained. The specific solution equation can refer to equation (12). In addition, the predicted model is compared with the measured model separately. If the model predictions meet the accuracy requirements, the corresponding model predictions of inlet pressure and hydrate saturation are output. If the prediction model accuracy is not met, the prediction model will continue to be optimized until the prediction accuracy is met and the relevant key parameters are output.

$$K = \frac{2PQL\mu}{A(P_i^2 - P_o^2)} \quad (11)$$

where K is the permeability ($\mu \text{ m}^2$), Q is the gas flux (ml/s), A is the cross-sectional area (cm^2), μ is the methane gas viscosity ($\text{mPa}\cdot\text{s}$), P_i and P_o are the inlet pressure (MPa) and outlet pressure (MPa) of the core respectively, and L is the length of the core (cm). P is the atmospheric pressure (MPa).

$$S_h = 1 - \left(\frac{2PQL\mu}{A(P_i^2 - P_o^2)K_0} \right)^{0.4} \quad (12)$$

The spatiotemporal dynamic evolution of the pressure distribution is analyzed on the basis of the results of the above logical derivation. As

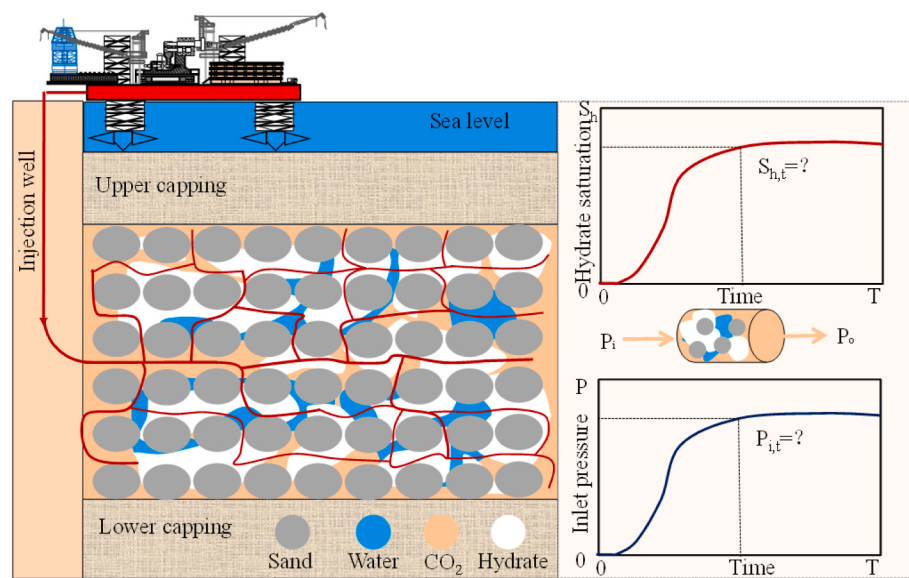


Fig. 11. Schematic diagram of CO₂ sequestration and injection process in hydrate method.

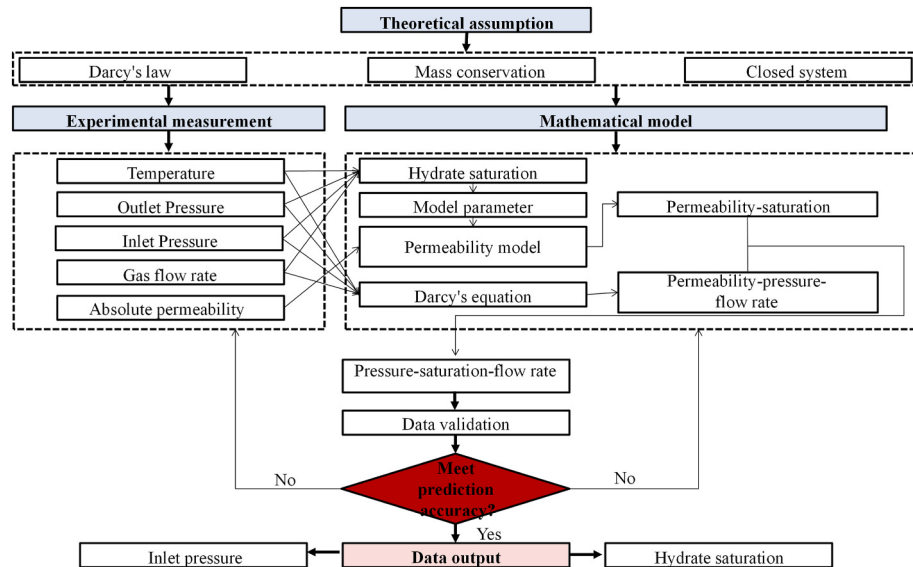


Fig. 12. Mathematical model development process and logical reasoning flowchart for key parameters.

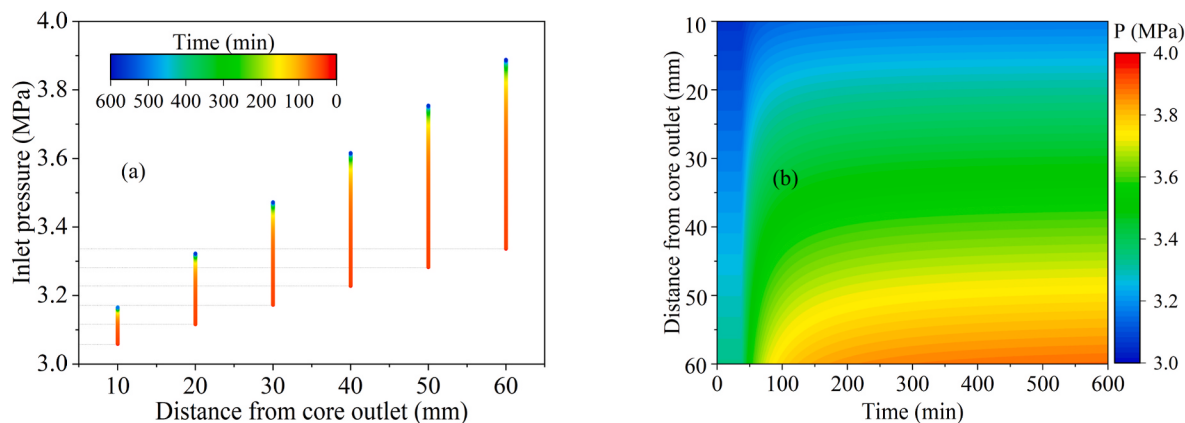


Fig. 13. Spatiotemporal distribution of reservoir pressure during gas flow.

illustrated in Fig. 13, the distribution of pressure is shown at different times and locations. Subsequently, the curves of hydrate formation are illustrated as an example for a gas flow rate of 0.03 ml/s. As demonstrated in Fig. 13(a), the gas pressure increases in proportion to the distance from the core outlet. The equation for calculating the gas pressure at different locations can be found in equation (13).

$$P_i = (2PQL\mu / (KA) + P_0^2)^{0.5} \quad (13)$$

At the initial moment, the inlet pressure is measured at 3.06 MPa, 3.12 MPa, 3.17 MPa, 3.23 MPa, 3.28 MPa, and 3.34 MPa at distances of 10 mm, 20 mm, 30 mm, 40 mm, 50 mm, and 60 mm from the core outlet, respectively. It is observed that the higher the distance from the core outlet, the higher the resistance to the flow of the gas, which requires higher inlet pressure to push the gas through the core. Similarly, the inlet pressure demonstrates an upward trend over time, which is primarily attributable to the continuous formation of hydrates (Park et al., 2023). To enhance the viability of inlet pressure prediction, the pressure cloud maps obtained through interpolation at varying spatiotemporal locations are presented in Fig. 13(b). The utilization of divergent color coding facilitates the discernment of varying pressure magnitudes. The pressure maps also demonstrate the induction time of hydrate formation, which is distributed around 35 min during the induction period of hydrate formation. The gas pressure remains constant during this time. The remolded core inlet pressure increases with increasing hydrate formation time and with greater distance from the core outlet.

Meanwhile, to verify the authenticity of the model data, a variety of experimental data are purposely selected as examples in this study. The analytical comparison between predicted and measured values is displayed in Fig. 14. In general, the predicted data better portray the dynamic evolution of the measured data. According to the design of experimental conditions in this study, the hydrate saturation at different flow rates and inlet pressures (equation (12)) satisfies equation (14). The outlet pressure is always kept at 3 MPa. In other words, the same design of experimental conditions as in this study, with different gas flow rates and inlet pressure input, can be used to achieve accurate prediction of hydrate saturation in hydrate-bearing cores in the flow regime. The gas flow rates and inlet pressures are directly accessible in practical working-condition applications.

$$S_h = (1 - 0.85 \cdot Q / (P_i^2 - 9))^0.4 \quad (14)$$

Furthermore, both the pressure and hydrate saturation of the

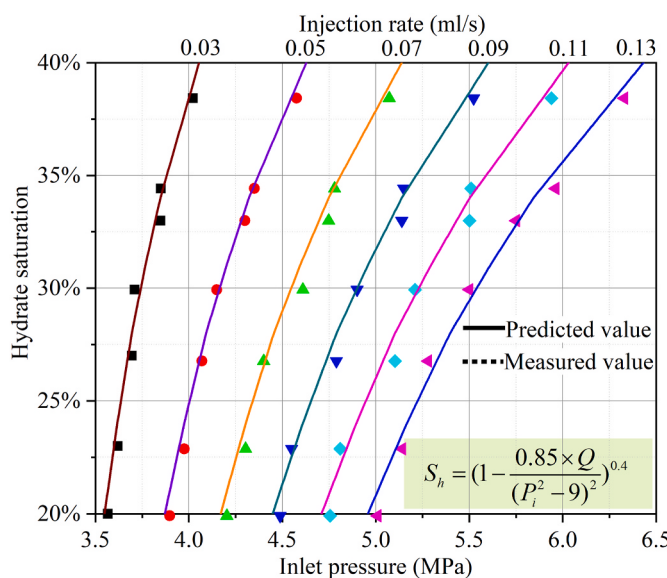


Fig. 14. Comparison of predicted and measured values for different in situ conditions.

remolded core in the flow regime are important parameters, and there is a coupled intrinsic relationship between them. Based on equation (12), it can be seen that the key parameters affecting the dynamic relationship between inlet pressure and hydrate saturation mainly include gas flow rate, distance from the core outlet, absolute permeability, and reservoir pressure (outlet pressure). The dynamic evolution curves between inlet pressure and hydrate saturation for different influencing parameters are displayed in Fig. 15. It is evident that the dynamic curves of inlet pressure and hydrate saturation, influenced by various parameters, do not coincide. However, a consistent tendency is observed: with an increase in inlet pressure, the predicted hydrate saturation data also rises. This increase in hydrate saturation is accompanied by an increase in inlet pressure. To enhance the comparability between different variables, the most fundamental settings in this study are as follows: reservoir pressure (outlet pressure) of 3 MPa, gas flow rate of 0.03 ml/s, core length of 6 cm, and initial permeability of 12 mD.

The inlet pressure-hydrate saturation curves for different gas flow rates are shown in Fig. 15(a). It is evident that as the gas flow rate is increased, the predicted hydrate saturation data decrease. This observation indicates a negative correlation between the two variables in the predicted relationship. At an inlet pressure of 5 MPa, the gas flow rate increases from 0.03 ml/s to 0.13 ml/s, while the hydrate saturation decreases from 56.62% to 19.91%. The predicted curves for different distances from the core exit distance are displayed in Fig. 15(b). With other conditions remaining constant, the further away from the outlet of the remolded core, the lower the predicted hydrate saturation. The distribution of predicted values under different conditions and the difference between them can be obtained based on the sparsity between the different curves. At low inlet pressures, the difference between the predicted saturation data at different distances is small. As the inlet pressure increases, the difference between the predicted saturation data at different distances becomes larger. At 3.5 MPa, the predicted hydrate saturation is 26.77%, 22.87%, and 17.21% at distances of 4 cm, 5 cm, and 6 cm from the core outlet, respectively. Similarly, at 4.5 MPa, the predicted hydrate saturation is 56.62%, 53.59%, and 47.52%, respectively.

The predicted data at different absolute permeabilities are summarized in Fig. 15(c). As the absolute permeability increases, the predicted hydrate saturation levels also increase. At an inlet pressure of 4.5 MPa, the predicted hydrate saturation is 53.59%, 50.55%, 47.52%, 44.49%, 38.43%, and 33.13% for initial permeabilities of 16 mD, 14 mD, 12 mD, 10 mD, 8 mD, and 6 mD, respectively. Similarly, the inlet pressure and hydrate saturation prediction curves for different reservoir pressures (outlet pressures) are shown separately in Fig. 15(d). The higher the reservoir pressure (outlet pressure), the smaller the hydrate saturation prediction data obtained. At an inlet pressure of 4 MPa and reservoir pressures (outlet pressure) of 2.9 MPa and 3.4 MPa, respectively, the difference in predicted saturation between the two is 14.69%. However, as the inlet pressure increases, the predicted hydrate saturation between different reservoir pressures (outlet pressure) gets closer. At an inlet pressure of 5 MPa and reservoir pressures (outlet pressures) of 2.9 MPa and 3.4 MPa, respectively, the difference in predicted saturation between the two is 6.07%.

4. Conclusions

The formation of hydrates during the geological storage of CO₂ by the hydrate method leads to a spatiotemporal dynamic evolution of permeability and pressure distribution in the remolded core. Consequently, the formation characteristics of hydrate formation, permeability, gas pressure, and saturation prediction at varying gas flow rates were investigated separately.

- (1) The formation parameters of hydrate at different CO₂ injection flow rates have been analyzed. Results indicate that lower flow rates lead to higher hydrate formation and greater water

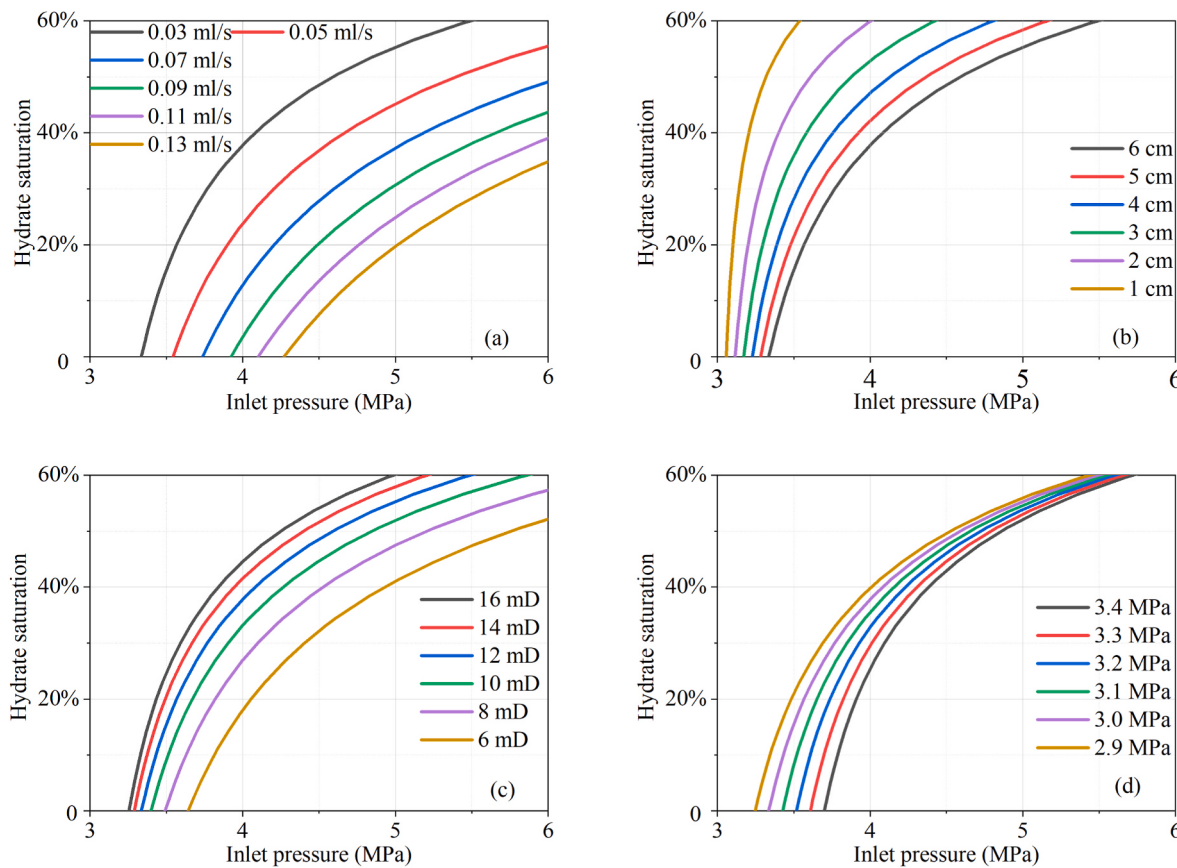


Fig. 15. Relationship between inlet pressure and predicted hydrate saturation for different in-situ conditions.

conversion rates but also prolong the induction time. A decrease in gas flow rate from 0.13 ml/s to 0.03 ml/s results in a 0.04 mol increase in hydrate formation and a 0.28 rise in water conversion, with the induction time extending by approximately 25 min.

- (2) A CO₂ hydrate dynamic formation prediction model and a permeability model were developed. The hydrate formation behavior during flow conforms to the prediction model $N(t) = N_0 \cdot e^{b/(t + c)}$, which effectively predicts hydrate dynamics at different flow rates, with correlation coefficients between measured and predicted values exceeding 92%. Parameters b and c both show linear relationships with gas flow rates, and are expressed as $b = -212.85\alpha Q - 5.80$ and $c = 0.89\beta Q + 0.013$, respectively.
- (3) The permeability and hydrate saturation under the present study conditions satisfy the permeability model $K = K_0(1 - S_h)^{2.5}$. The presence of hydrate reduces the permeability of the core. The increase of hydrate saturation from 0 to 34.42% corresponds to a permeability measurement of 4.17 mD, which is 7.83 mD lower than the initial permeability.
- (4) The dynamic spatiotemporal distribution prediction of gas pressure and hydrate saturation within the core during flow was achieved. Hydrate formation has a significant effect on the inlet pressure and maintains a positive correlation. Coupled with the permeability model and Darcy's law, the spatiotemporal evolution of gas pressure and hydrate saturation has been logically derived. Hydrate saturation decreases as the gas flow rate, distance from the core outlet, and reservoir pressure (outlet pressure) increase at constant inlet pressure. Conversely, hydrate saturation increases with higher absolute permeability at the same inlet pressure.

The results of this study can provide valuable insights into addressing

the "black box" problem in the practical engineering application of CO₂ geological storage, enabling dynamic optimization. The coupled prediction at the experimental scale offers an important theoretical foundation for predicting the spatiotemporal distributions of gas pressure and hydrate saturation during the actual engineering gas flow process. Future research should focus on enhancing the applicability and reliability of the prediction model in complex hydrate reservoirs under stress-coupled conditions.

CRediT authorship contribution statement

Jingru Zhang: Writing – review & editing, Writing – original draft, Investigation. **Ke Chen:** Investigation, Conceptualization. **Guangjun Gong:** Visualization, Investigation. **Yi Zhang:** Funding acquisition, Conceptualization. **Yongchen Song:** Supervision.

Declaration of competing interest

We declare no conflict of interest.

Acknowledgements

This work was supported by National Key Research and Development Program of China (2023YFB4104200), Liaoning Foundation Research Projects for Application (Grant 2023JH2/101300005), National Natural Science Foundation of China (Grant 51976024, 52076030).

Data availability

Data will be made available on request.

References

- Aghajanloo, M., Yan, L., Berg, S., Voskov, D., Farajzadeh, R., 2024. Impact of CO₂ hydrates on injectivity during CO₂ storage in depleted gas fields: a literature review. *Gas Sci. Eng.* 123, 205250.
- Ahmad, S., Li, Y.M., Li, X.F., Xia, W., Chen, Z., Wang, P., 2020. Modeling of CO₂ storage as hydrate in vacated natural gas hydrate formation. *Int. J. Energy Res.* 44, 528–547.
- Aminnaji, M., Qureshi, M.F., Dashti, H., Hase, A., Mosalanejad, A., Jahanbakhsh, A., et al., 2024. CO₂ gas hydrate for carbon capture and storage applications. *Energy* 300, 131580.
- Bashir, A., Ali, M., Patil, S., Aljawad, M.S., Mahmoud, M., Al-Shehri, D., et al., 2024. Comprehensive review of CO₂ geological storage: exploring principles, mechanisms, and prospects. *Earth Sci. Rev.* 249, 104672.
- Dashti, H., Yew, L.Z., Lou, X., 2015. Recent advances in gas hydrate-based CO₂ capture. *J. Nat. Gas Sci. Eng.* 23, 195–207.
- Eigbe, P.A., Ajayi, O.O., Olakoyejo, O.T., Fadipe, O.L., Efe, S., Adelaja, A.O., 2023a. A general review of CO₂ sequestration in underground geological formations and assessment of depleted hydrocarbon reservoirs in the niger Delta. *Appl. Energy* 350, 121723.
- Eigbe, P.A., Ajayi, O.O., Olakoyejo, O.T., Fadipe, O.L., Efe, S., Adelaja, A.O., 2023b. A general review of CO₂ sequestration in underground geological formations and assessment of depleted hydrocarbon reservoirs in the niger Delta. *Appl. Energy* 350.
- Englezos, P., Kalogerakis, N., Dholabhai, P.D., Bishnoi, P.R., 1987. Kinetics of formation of methane and ethane gas hydrates. *Chem. Eng. Sci.* 42, 2647–2658.
- Gong, G., Zhao, G., Pang, W., Tian, M., Chen, B., Yang, M., et al., 2023. Continuous measurement of gas permeability in non-homogeneous hydrate reservoirs under effective pressure via a novel apparatus. *Gas Sci. Eng.* 118, 205091.
- Gong, G., Yang, M., Pang, W., Zheng, J-n., Song, Y., 2024. Dynamic optimization of real-time depressurization pathways in hydrate-bearing south sea clay reservoirs. *Energy* 292, 130446.
- Gong, G.J., Zhang, J.R., Zheng, J.N., Zhao, G.J., Pang, W.X., Song, Y.C., et al., 2025. Formation kinetics and MRI visualization of CO₂ hydrate with different flow conditions in porous media: evolution prediction model of stored CO₂ leakage. *Energy* 327.
- Guo, Y., Li, S., Sun, H., Wu, D., Liu, L., Zhang, N., et al., 2024. Enhancing gas production and CO₂ sequestration from marine hydrate reservoirs through optimized CO₂ hydrate cap. *Energy* 303, 131821.
- Junji, yamaguchi A., Sato, T., Tobase, T., Wei, X., Huang, L., Zhang, J., et al., 2023. Multiscale numerical simulation of CO₂ hydrate storage using machine learning. *Fuel*, 126678.
- Kuang, Y., Zhang, L., Zheng, Y., 2022. Enhanced CO₂ sequestration based on hydrate technology with pressure oscillation in porous medium using NMR. *Energy* 252, 124082.
- Kumar, Y., Ghoderao, M., Sarkhel, R., Sangwai, J., 2024. Exploring CO₂ sequestration potential as gas hydrates in clay dominated subsea system with and without surfactant. *Fuel* 363, 130990.
- Lijith, K.P., Rao, R.S., Singh, D.N., 2024. Detection of formation and dissociation of CO₂ hydrates in fine-sands through acoustic waves. *Fuel* 357, 129802.
- Lu, S.Y., Yamaguchi, A.J., Kobayashi, K., Sato, T., Tobase, T., 2022. Numerical simulation of microscopic CO₂ hydrate formation in sandy sediment with two-phase flow. *Int. J. Greenh. Gas Control* 121, 103789.
- Macreadie, P.I., Anton, A., Raven, J.A., Beaumont, N., Connolly, R.M., Friess, D.A., et al., 2019. The future of blue carbon science. *Nat. Commun.* 10, 3998.
- Meyer, D.W., Flemings, P.B., DiCarlo, D., You, K.H., Phillips, S.C., Kneafsey, T.J., 2018. Experimental investigation of gas flow and hydrate formation within the hydrate stability zone. *J. Geophys. Res. Solid Earth* 123, 5350–5371.
- Munkejord, S.T., Hammer, M., Lovseth, S.W., 2016. CO₂ transport: data and models - a review. *Appl. Energy* 169, 499–523.
- Mwakipunda, G.C., Mgimba, M.M., Ngata, M.R., Yu, L., 2024. Recent advances on carbon dioxide sequestration potentiality in salt caverns: a review. *Int. J. Greenh. Gas Control* 133, 104109.
- Ouyang, Q., Zheng, J., Pandey, J.S., von Solms, N., Linga, P., 2024. Coupling amino acid injection and slow depressurization with hydrate swapping exploitation: an effective strategy to enhance in-situ CO₂ storage in hydrate-bearing sediment. *Appl. Energy* 366, 123300.
- Park, J.H., Park, J., Lee, J.W., Kang, Y.T., 2023. Progress in CO₂ hydrate formation and feasibility analysis for cold thermal energy harvesting application. *Renew. Sustain. Energy Rev.* 187, 113783.
- Qi, Y., Sun, Y., Li, B., Shan, H., Shen, Y., Zhang, G., 2023. Permeability damage and hydrate dissociation barrier caused by invaded fracturing fluid during hydrate reservoir stimulation. *Gas Sci. Eng.* 116, 205051.
- Sigman, D.M., Hain, M.P., Haug, G.H., 2010. The polar ocean and glacial cycles in atmospheric CO₂ concentration. *Nature* 466, 47–55.
- Stolwijk, J.J., Mehrmann, V., 2018. Error analysis and model adaptivity for flows in gas networks. *Analele Stiintifice Ale Universitatii Ovidius Constanta-Seria Matematica*. 26, 231–266.
- Sun, S., Gu, L., Yang, Z., Lin, H., Li, Y., 2023. Hydrate formation from CO₂ saturated water under displacement condition. *Renew. Sustain. Energy Rev.* 179, 113293.
- Tongu, D., Obara, Sy, 2024. Formation temperature range expansion and energy storage properties of CO₂ hydrates. *Renew. Sustain. Energy Rev.* 189, 113971.
- Wang, P.F., Wang, S.L., Song, Y.C., Yang, M.J., 2018. Dynamic measurements of methane hydrate formation/dissociation in different gas flow direction. *Appl. Energy* 227, 703–709.
- Wang, X., Liang, B., Wang, F., Sun, W.J., Yang, X.L., Ma, G.Y., et al., 2024. An improved phase equilibrium model for methane hydrate dissociation inside pore. *Appl. Energy* 368.
- Weng, H., Liu, Z., Wang, D., 2023. Alpha model: a C plus plus code for modelling and analyzing hydrate-saturation-dependent permeability of hydrate-bearing porous media. *SoftwareX* 23, 101433.
- Yamada, K., Fernandes, B.R.B., Kalamkar, A., Jeon, J., Delshad, M., Farajzadeh, R., et al., 2024. Development of a hydrate risk assessment tool based on machine learning for CO₂ storage in depleted gas reservoirs. *Fuel* 357, 129670.
- Yin, Z.Y., Khurana, M., Tan, H.K., Linga, P., 2018. A review of gas hydrate growth kinetic models. *Chem. Eng. J.* 342, 9–29.
- Zhang, L.X., Yang, L., Wang, J.Q., Zhao, J.F., Dong, H.S., Yang, M.J., et al., 2017. Enhanced CH₄ recovery and CO₂ storage via thermal stimulation in the CH₄/CO₂ replacement of methane hydrate. *Chem. Eng. J.* 308, 40–49.
- Zhao, J., Zheng, J.N., Kang, T.Q., Chen, B.B., Yang, M.J., Song, Y.C., 2021. Dynamic permeability and gas production characteristics of methane hydrate-bearing marine muddy cores: experimental and modeling study. *Fuel* 306, 121630.
- Zhao, G., Zheng, J-n., Gong, G., Chen, B., Yang, M., Song, Y., 2023. Formation characteristics and leakage termination effects of CO₂ hydrate cap in case of geological sequestration leakage. *Appl. Energy* 351, 121896.
- Zhu, M., Chen, L., Su, S., Hu, S., Xu, K., Yan, P.W., et al., 2022. Flow resistance analysis of non-isothermal supercritical CO₂. *Appl. Therm. Eng.* 215, 119022.